PPARγ Deacetylation Confers the Antiatherogenic Effect and Improves Endothelial Function in Diabetes Treatment

Longhua Liu,[1,2] Lihong Fan,[1,2,3] Michelle Chan,[4] Michael J. Kraakman,[1,5] Jing Yang,[1,2,6] Yong Fan,[1,2] Nicole Aaron,[1,7] Qianfen Wan,[1,2] Maria Alicia Carrillo-Sepulveda,[8] Alan R. Tall,[5] Ira Tabas,[5] Domenico Accili,[1,5] and Li Qiang[1,2]

Diabetes 2020;69:1793–1803 | https://doi.org/10.2337/db20-0217

Cardiovascular disease (CVD) is the leading cause of death in patients with diabetes, and tight glycemic control fails to reduce the risk of developing CVD. Thiazolidinediones (TZDs), a class of peroxisome proliferator–activated receptor γ (PPARγ) agonists, are potent insulin sensitizers with antiatherogenic properties, but their clinical use is limited by side effects. PPARγ deacetylation on two lysine residues (K268 and K293) induces brown remodeling of white adipose tissue and uncouples the adverse effects of TZDs from insulin sensitization. Here we show that PPARγ deacetylation confers antiatherogenic properties and retains the insulin-sensitizing effects of TZD while circumventing its detriments. We generated mice homozygous with mice with deacetylation-mimetic PPARγ mutations K268R/K293R (2KR) on an LDL-receptor knockout (*Ldlr*$^{-/-}$) background. *2KR:Ldlr*$^{-/-}$ mice showed smaller atherosclerotic lesion areas than *Ldlr*$^{-/-}$ mice, particularly in aortic arches. With rosiglitazone treatment, *2KR:Ldlr*$^{-/-}$ mice demonstrated a residual antiatherogenic response and substantial protection against bone loss and fluid retention. The antiatherosclerotic effect of 2KR was attributed to the protection of endothelium, indicated by improved endothelium-dependent vasorelaxation and repressed expression of proatherogenic factors including inducible nitric oxide synthase, interleukin-6, and NADPH oxidase 2. Therefore, manipulating PPARγ acetylation is a promising therapeutic strategy to control risk of CVD in diabetes treatment.

Cardiovascular disease (CVD) is the leading cause of death worldwide and accounts for ∼40% of deaths and ∼50% of health care expenses among patients with type 2 diabetes (T2D) (1,2). Atherosclerosis is associated with a two- to fourfold increase in morbidity and mortality among patients with T2D (1). However, tight glycemic control is not effective in preventing and treating CVD in patients with T2D (3). The only insulin-sensitizing antidiabetes drugs currently available are thiazolidinediones (TZDs), synthetic ligands of peroxisome proliferator–activated receptor γ (PPARγ). As a nuclear receptor, PPARγ heterodimerizes with retinoid X receptor in response to ligand binding and binds to sequence-specific DNA motifs to regulate gene expression (4). PPARγ is primarily expressed in adipocytes (5) and, to a lesser extent, in various tissues (6). PPARγ has both anti-inflammatory and antiatherogenic effects, and activation of PPARγ by TZDs inhibits atherosclerosis in male *Ldlr*$^{-/-}$ mice (7). The antiatherogenic effects of PPARγ seem to be mediated by its actions in macrophages, vascular endothelial cells, and smooth muscle cells (7–9). In the Insulin Resistance Intervention after Stroke (IRIS) trial, patients without diabetes but with a recent history of ischemic stroke and insulin resistance who were treated with pioglitazone showed a 24% lower risk of stroke or myocardial infarction and a 52% lower incidence of diabetes than those in the placebo group (10). Nevertheless, these improvements in CVD were

[1]Naomi Berrie Diabetes Center, Columbia University, New York, NY
[2]Department of Pathology and Cell Biology, Columbia University, New York, NY
[3]Department of Cardiology, The First Affiliated Hospital of Xi'an Jiao Tong University, Xi'an, Shanxi, China
[4]Department of Biological Sciences, Columbia University, New York, NY
[5]Department of Medicine, Columbia University, New York, NY
[6]Department of Endocrinology, The First Affiliated Hospital of Xi'an Jiao Tong University, Xi'an, Shanxi, China
[7]Department of Pharmacology, Columbia University, New York, NY
[8]Department of Biomedical Sciences, College of Osteopathic Medicine, New York Institute of Technology, Old Westbury, NY

Corresponding author: Li Qiang, lq2123@cumc.columbia.edu

Received 3 March 2020 and accepted 11 May 2020

This article contains supplementary material online at https://doi.org/10.2337/figshare.12280772.

L.L. and L.F. contributed equally.

overridden by detrimental effects such as weight gain, edema, and fragility fractures (11,12).

The safety profile of PPARγ agonists is postulated to be improved through the selective activation of subsets of PPARγ targets. Cues have emerged from studies of PPARγ posttranslational modifications, including acetylation, phosphorylation (13,14), SUMOylation (15), and *O*-GlcNAcylation (16), all of which differentially modulate PPARγ activity. Short-term treatment with the partial agonist SR1664, inhibiting Ser273 phosphorylation of PPARγ, in *ob/ob* mice improves insulin sensitivity without reducing hematocrit (17), whereas the PPARγ antagonist SR10171 inhibits Ser273 phosphorylation and increases bone mass (18). We have shown that PPARγ is deacetylated by the NAD^+-dependent deacetylase SirT1 and that TZDs promote PPARγ deacetylation on two lysine residues (K268 and K293) to induce brown remodeling of white adipose tissue (WAT) (19). Mice that are homozygous for amino acid substitutions mimicking the constitutively deacetylated state (K268R and K293R [2KR]) are protected against high-fat diet (HFD)–induced weight gain and its metabolic consequences (20). More importantly, the 2KR mutation maintains the insulin-sensitizing response to rosiglitazone without causing bone loss, weight gain, fluid retention, or cardiac hypertrophy following chronic treatment (20). On the basis of these data, we posited that targeting PPARγ acetylation can achieve the long-sought goal of separating the therapeutic benefits from the adverse consequences of PPARγ activation.

Given the antiatherogenic effect of TZDs, in this study we asked whether targeting PPARγ acetylation, specifically by 2KR mutation, could fulfill the prerequisite of controlling CVD in diabetes treatment. We found that homozygosity for the 2KR allele backcrossed onto an LDL receptor knockout background ($Ldlr^{-/-}$) conferred a basal antiatherogenic effect and retained TZD responsiveness without causing bone loss and fluid retention. We further demonstrated that the antiatherogenic effect was associated with increased vascular relaxation and endothelial function, suggesting an endothelium-dependent mechanism.

RESEARCH DESIGN AND METHODS

Animal Studies

2KR mice on a C57BL/6 background were generated as described previously (20). 2KR mice were bred with $Ldlr^{-/-}$ mice on a C57BL/6 background. Mice were housed at 23 ± 1°C under a 12-h light/12-h dark cycle, with access to food and water ad libitum. The mice were fed a Western-type diet (WTD) containing 42% calories from fat, 15.2% from protein, and 42.7% from carbohydrates, as well as 0.2% cholesterol (TD.88137; Envigo). Rosiglitazone maleate (Avandia; 100 mg/kg) (ab142461; Abcam) was mixed into the WTD to achieve a dose of ∼5 mg/kg body weight (BW). For an intraperitoneal glucose tolerance test, mice were deprived of food overnight (16 h) in cages with fresh bedding, and then injected i.p. with glucose (2.0 g/kg BW). For the insulin tolerance test, mice were deprived of food for 4 h and then injected i.p. with insulin (0.75 units/kg BW). A Breeze2 glucometer (Bayer) was used to measure blood glucose at various time points. Body composition was determined by using the EchoMRI analyzer. Liver triglycerides (TGs) were extracted as previously described (21). Plasma parameters were measured with Mouse Insulin ELISA (Mercodia), Infinity Triglycerides Liquid Stable Reagent (Thermo Fisher Scientific), HR Series NEFA-HR (Fujifilm Wako), total cholesterol (Fujifilm Wako), and HDL-Cholesterol E (Fujifilm Wako). All animal protocols used in this study were reviewed and approved by the Columbia University Animal Care and Utilization Committee.

Fast-Protein Liquid Chromatography

Plasma samples (20 μL) from wild-type (WT) and 2KR mice were diluted 10 times with PBS and then loaded onto a Superdex 200 Increase 10/300GL fast-protein liquid chromatography (FPLC) column (28990944; GE Healthcare). The elution was performed with FPLC buffer (100 mmol/L Tris, 0.4 g/L NaN_3 [pH 7.5]) at a flow speed of 0.3 mL/min. The collected fractions (0.25 mL each) were freshly assayed to determine cholesterol and TG levels.

Analyses of Atherosclerotic Lesions in Mouse Aortic Arches and Roots

Mice (10–12 weeks old) were fed the WTD or the WTD with rosiglitazone for 8 or 12 weeks. For tissue collection, mice were euthanized with CO_2. Blood was drawn through a left ventricular puncture for later use, followed by perfusion with cold PBS. Aortae were dissected, and aortic arches were photographed. The aortae then were fixed in paraformaldehyde, and plaques were quantified by Oil Red O en face staining. ImageJ software was used to quantify the area of the atherosclerotic lesion. For analysis of aortic root lesions, aortic roots were fixed in paraformaldehyde and embedded in paraffin. Serial sections (6 μm each) were obtained, and six paraffin sections, 60 μm apart, were stained with Harris hematoxylin and eosin (H&E). The areas of aortic lesions and necrotic core were quantified on the basis of established methods (22).

Bone Processing and Analysis

Femurs were collected and fixed in 10% neutral buffered formalin at 4°C overnight, and they were subsequently processed for bone microarchitecture analysis and lipid quantification by using a Quantum FX micro–computed tomography (CT) scanner (PerkinElmer). For lipid quantification, the bones were submerged in the 14% EDTA solution for at least 2 weeks to decalcify them, and then were stained in a 1% osmium tetroxide and 2.5% potassium dichromate solution at room temperature for 48 h, washed in tap water for at least 2 h, and then imaged by micro-CT. Analyze 12.0 software was used to quantify micro-CT scan parameters and lipid volumes.

Vascular Reactivity

Thoracic aortae were isolated and carefully cleared of perivascular fat and adventitia in oxygenated Krebs buffer (130 mmol/L NaCl, 14.9 mmol/L $NaHCO_3$, 4.7 mmol/L KCl, 1.18 mmol/L KH_2PO_4, 1.17 mmol/L $MgSO_4$-$7H_2O$, 1.56 mmol/L $CaCl_2$-$2H_2O$, 0.026 mmol/L EDTA, 5.5 mmol/L glucose [pH 7.4]). Thoracic aortae then were cut into rings (2 mm long) and mounted on a Multi-Wire Myograph System 620M (Danish Myo Technology, Aarhus, Denmark) to record isometric tension by using a PowerLab 8/35 data acquisition system (ADInstruments Pty Ltd., Castle Hill, Australia). Aortic rings were equilibrated in Krebs buffer (74.7 mmol/L NaCl, 14.9 mmol/L $NaHCO_3$, 60 mmol/L KCl, 1.18 mmol/L KH_2PO_4, 1.17 mmol/L $MgSO_4$-$7H_2O$, 1.6 mmol/L $CaCl_2$-$2H_2O$, 0.026 mmol/L EDTA, 5.5 mmol/L glucose) for 30 min and then perfused through the chambers with 5% CO_2 and 95% O_2 at 37°C, as previously described (23). In all experiments, aortic ring integrity was assessed by stimulation with 120 mmol/L KCl. For testing the presence of endothelium, segments were contracted with 1 μmol/L phenylephrine (PE) (Sigma Aldrich, St. Louis, MO); upon reaching a stable maximum tension, the vessels were stimulated with 10 μmol/L acetylcholine (ACh) (Sigma Aldrich), and relaxation was confirmed. Aortic rings that responded with >80% relaxation were considered to have a preserved endothelium. Cumulative concentration-response curves for Ach (1 nmol/L to 10 μmol/L) and sodium nitroprusside (SNP) (1 nmol/L to 10 μmol/L) were obtained to assess endothelium-dependent and -independent relaxation responses, respectively.

Aortic Histomorphometric Analysis

Cryosections of aortae (5 μm each) were mounted on slides, fixed in 10% formalin, and stained with H&E (Sigma Aldrich). High-resolution bright field and fluorescent light digital images were captured by using an Olympus IX71 microscope equipped with a DP73 camera. Morphometric data—specifically cross-sectional area and wall-to-lumen ratio of the aortae—were obtained by using ImageJ software (National Institutes of Health).

Quantitative Real-Time PCR

Tissues and cells were lysed with 1 mL TRIzol reagent (Thermo Fisher Scientific). After separating phases through the addition of 200 μL chloroform, RNA was isolated by using a NucleoSpin RNA Kit (Macherey-Nagel, Inc.). An Applied Biosystems High-Capacity cDNA Reverse Transcription Kit (Thermo Fisher Scientific) was used to synthesize cDNA from 1 μg total RNA. Quantitative PCR was performed on a Bio-Rad CFX96 Touch Real-Time PCR Detection System with the GoTaq qPCR Master Mix (Promega). Relative gene expression was calculated by using the ΔΔCt method, with *Rpl23* as the reference gene.

Western Blotting

Cells were lysed and tissues were homogenized in a Polytron homogenizer immediately after dissection in Western

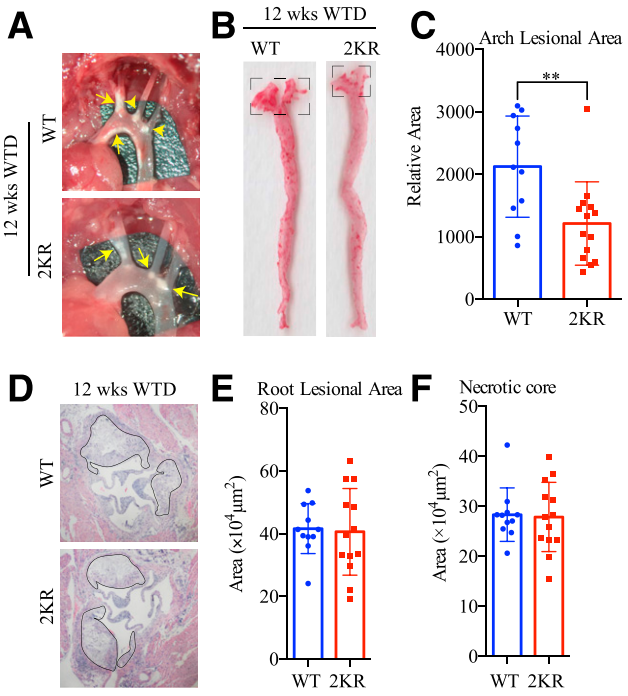

Figure 1—PPARγ deacetylation inhibits aortic arch atherosclerosis. Male mice on an *Ldlr*$^{-/-}$ background (11 WT and 14 2KR mice) were fed the WTD for 12 weeks (wks). *A*: Representative images of aortic arches. The yellow arrows indicate plaques. $^{**}P < 0.01$, two-tailed Mann-Whitney *U* test. *B*: En face aortic plaque analysis with Oil Red O staining. The quantified arch lesion areas are shown in the dashed squares. *C*: Quantification of aortic arch plaque areas. *D*: Representative H&E staining of aortic root sections. Plaques are outlined in black. *E* and *F*: Quantification of total lesion area (*E*) and necrotic core area (*F*) of aortic root sections. Data in *C*, *E*, and *F* are presented as the mean ± SEM.

extraction buffer (150 mmol/L NaCl, 10% glycerol, 1% NP-40, 1 mmol/L EDTA, 20 mmol/L NaF, 30 mmol/L sodium pyrophosphate, 0.5% sodium deoxycholate, 0.05% SDS, 25 mmol/L Tris-HCl [pH 7.4]) containing a protease inhibitor cocktail (Roche). The lysate was sonicated and incubated on ice for 30 min before centrifugation. SDS-PAGE and Western blotting were performed and detected with enhanced chemiluminescence (32106; Thermo Fisher Scientific). The antibodies were anti-Nox2 antibody (SAB4300724; Sigma-Aldrich) and anti-GAPDH antibody (HRP-60004; Proteintech Group, Inc.).

Statistical Analysis

Values are presented as the mean ± SEM. Statistical significance was determined by using the Mann-Whitney *U* test for quantifying the aortic lesional area and necrotic core. The Student *t* test was used for statistical analyses of data from two groups. Two-way ANOVA was used to compare difference between groups with two independent variables. Concentration-response curves were log transformed, normalized to the percentage of maximal response, and fitted by using a nonlinear interactive fit. All data were analyzed in GraphPad Prism software version 7 (GraphPad Software, San Diego, CA).

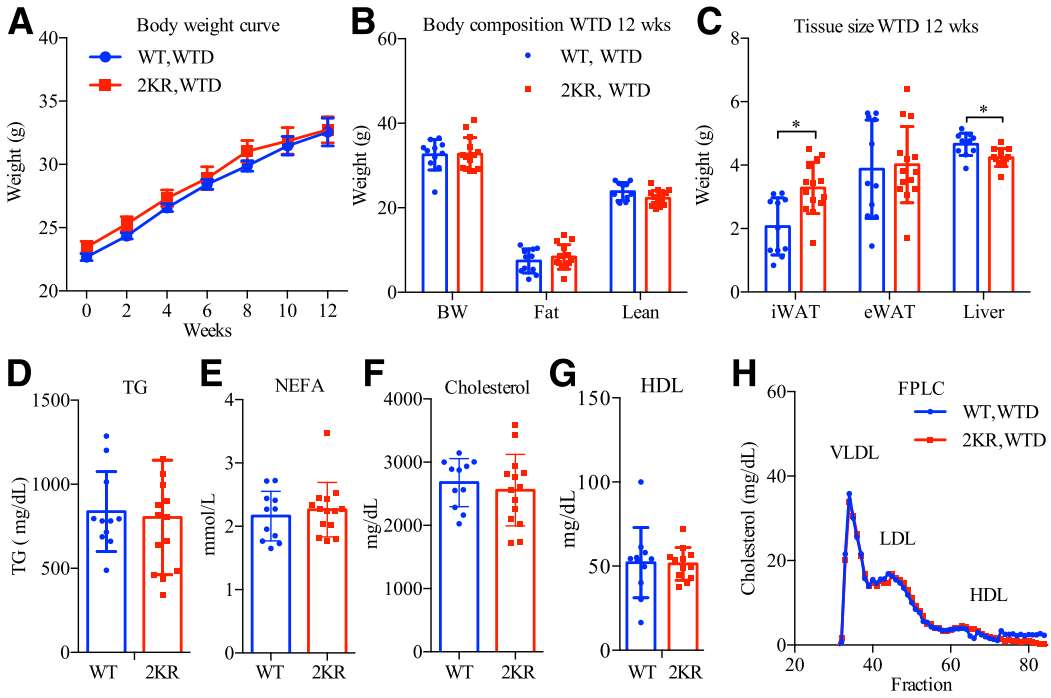

Figure 2—The antiatherogenic effect of 2KR is independent of plasma cholesterol and lipid levels. Male mice on an *Ldlr*$^{-/-}$ background (11 WT and 14 2KR mice) were fed the WTD for 12 weeks. *A*: Body-weight curve over the duration of WTD feeding. *B* and *C*: Body composition (*B*) and tissue sizes (*C*) after 12 weeks (wks) of eating the WTD. *D*–*G*: Plasma TG (*D*), NEFA (*E*), total cholesterol (*F*), and HDL cholesterol (*G*) levels. *H*: Size-fractionation of lipoproteins by FPLC. *$P < 0.05$, two-sided Student *t* test. Data are presented as the mean ± SEM. eWAT, epididymal white adipose tissue; iWAT, inguinal white adipose tissue.

Data and Resource Availability

All relevant data are provided within this article, and all data sets are available on reasonable request.

RESULTS

Reduced Aortic Arch Lesions in *2KR:Ldlr*$^{-/-}$ Mice

To investigate whether PPARγ deacetylation confers antiatherogenic effects, we backcrossed the PPARγ deacetylation-mimetic 2KR mutant allele onto the LDL receptor knockout (*Ldlr*$^{-/-}$) background. Three-month-old male *2KR:Ldlr*$^{-/-}$ mice and control *Ldlr*$^{-/-}$ littermates were fed a WTD for 12 weeks to allow us to evaluate atherosclerosis. *2KR:Ldlr*$^{-/-}$ mice showed fewer aortic arch plaques (Fig. 1*A*) and a >40% smaller aortic arch lesion area than seen in *WT:Ldlr*$^{-/-}$ mice (Fig. 1*B* and *C*). In contrast, areas of aortic root lesions and necrotic core were the same between the genotypes (Fig. 1*D*–*F*). The inhibition of arch lesion progression was initiated early during atherosclerosis. As early as 8 weeks after WTD consumption, *2KR:Ldlr*$^{-/-}$ mice displayed an ∼30% reduction in aortic arch lesion area without a significant decrease in aortic root lesion and necrotic core areas (Supplementary Fig. 1*A*–*F*). Similarly, female *2KR:Ldlr*$^{-/-}$ mice showed a consistent decrease (by ∼30%) of the arch lesion area after 12 weeks of eating the WTD (Supplementary Fig. 2*A*–*C*). These results indicate that PPARγ deacetylation protects against atherosclerotic lipid accumulation, specifically in the aortic arch.

The Antiatherogenic Effect of 2KR Is Independent of Plasma Cholesterol and Lipid Levels

To understand the antiatherogenic effect of PPARγ deacetylation, we assessed various metabolic parameters. Despite gaining a similar amount of weight and having a similar body composition to *WT:Ldlr*$^{-/-}$ mice upon eating the WTD (Fig. 2*A* and *B*), *2KR:Ldlr*$^{-/-}$ mice had larger inguinal WAT depot sizes accompanied by smaller livers (Fig. 2*C*), mimicking a TZD-like effect of promoting TG storage and lipid partitioning in adipose tissue rather than liver (24). However, there was no significant improvement of liver steatosis, as determined by liver TG content and liver morphology (Supplementary Fig. 3*A* and *B*). These two groups of mice had comparable levels of plasma TGs, nonesterified fatty acids (NEFAs), total cholesterol (Fig. 2*D*–*F*), and HDL, LDL, and VLDL cholesterol after 12 weeks of eating the WTD (Fig. 2*G* and *H*). These findings were largely replicated in female mice, although HDL cholesterol levels were higher (Supplementary Fig. 2*E*–*K*), which may account for their more pronounced antiatherogenic phenotype (25,26). These data collectively suggest that the antiatherogenic effect of 2KR is not likely to be attributable to differences in systemic metabolic changes.

2KR:Ldlr$^{-/-}$ Mice Preserve the Antiatherogenic Effect Upon Rosiglitazone Treatment

Next, we investigated whether the antiatherogenic effect is preserved in mutant mice when they are treated with

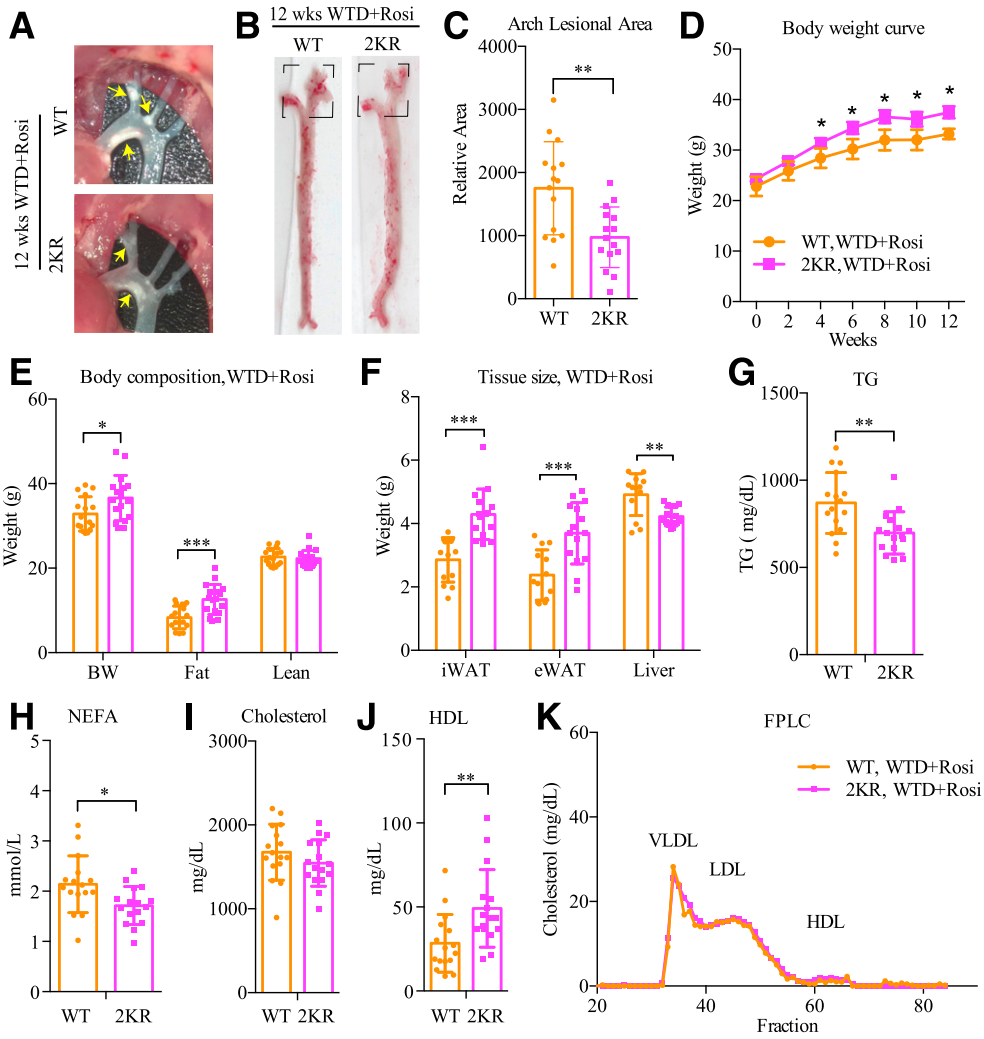

Figure 3—PPARγ deacetylation preserves the antiatherogenic effect in the aortic arch with rosiglitazone treatment. Male mice on an *Ldlr*$^{-/-}$ background (15 WT and 15 2KR mice) were fed the WTD with rosiglitazone (WTD+Rosi) for 12 weeks. *A*: Representative images of aortic arches. Yellow arrows indicate plaques. *B*: En face aortic plaque analysis with Oil Red O staining. The quantified arch lesion areas are set within dashed squares. *C*: Quantification of aortic arch plaque areas. $^{**}P < 0.01$, two-tailed Mann-Whitney *U* test. *D*: Body-weight curve over the duration of WTD+Rosi. *E* and *F*: Body composition (*E*) and tissue sizes (*F*) after WTD+Rosi. *G*–*J*: Plasma TG (*G*), NEFA (*H*), total cholesterol (*I*), and HDL cholesterol (*J*) levels. $^{*}P < 0.05$, $^{**}P < 0.01$, $^{***}P < 0.001$, two-sided Student *t* test. Data are presented as the mean ± SEM. eWAT, epididymal white adipose tissue; iWAT, inguinal white adipose tissue.

rosiglitazone, which, unlike pioglitazone, has no PPARα agonism (27). After 12 weeks of eating the WTD with rosiglitazone, *2KR:Ldlr*$^{-/-}$ mice retained the >40% smaller aortic arch lesion area than *T:Ldlr*$^{-/-}$ (Fig. 3*A*–*C*). *2KR:Ldlr*$^{-/-}$ mice gained slightly more weight than *WT:Ldlr*$^{-/-}$ mice upon rosiglitazone treatment as a result of increased adiposity contributed by both inguinal WAT and epididymal WAT; however, their livers remained smaller (Fig. 3*D*–*F*). Consistent with increased lipid storage in adipocytes, *2KR:Ldlr*$^{-/-}$ mice had lower circulating TG and NEFA levels (Fig. 3*G* and *H*), but similar levels of total cholesterol, VLDL cholesterol, and LDL cholesterol (Fig. 3*I*–*K*). Interestingly, *2KR:Ldlr*$^{-/-}$ mice resisted the rosiglitazone-induced decrease of HDL cholesterol (Fig. 3*J* vs. Fig. 2*G*). These data collectively suggest that PPARγ deacetylation procures the benefits of inhibiting atherosclerosis, which may be contributed by the improved cholesterol and lipid metabolism, upon rosiglitazone treatment.

Insulin-Sensitizing Actions of Rosiglitazone in *2KR:Ldlr*$^{-/-}$ Mice

Both male and female *2KR:Ldlr*$^{-/-}$ and *WT:Ldlr*$^{-/-}$ mice fed the WTD showed similar glucose tolerance, insulin sensitivity, and plasma insulin levels (Fig. 4 and Supplementary Fig. 2*L*–*N*). We investigated their responses to TZD. As expected, rosiglitazone significantly improved glucose tolerance and insulin sensitivity in *WT:Ldlr*$^{-/-}$ mice and to a lesser extent in *2KR:Ldlr*$^{-/-}$ mice (Fig. 4*A*–*D*). The reduced response to rosiglitazone in *2KR:Ldlr*$^{-/-}$ mice is in line with

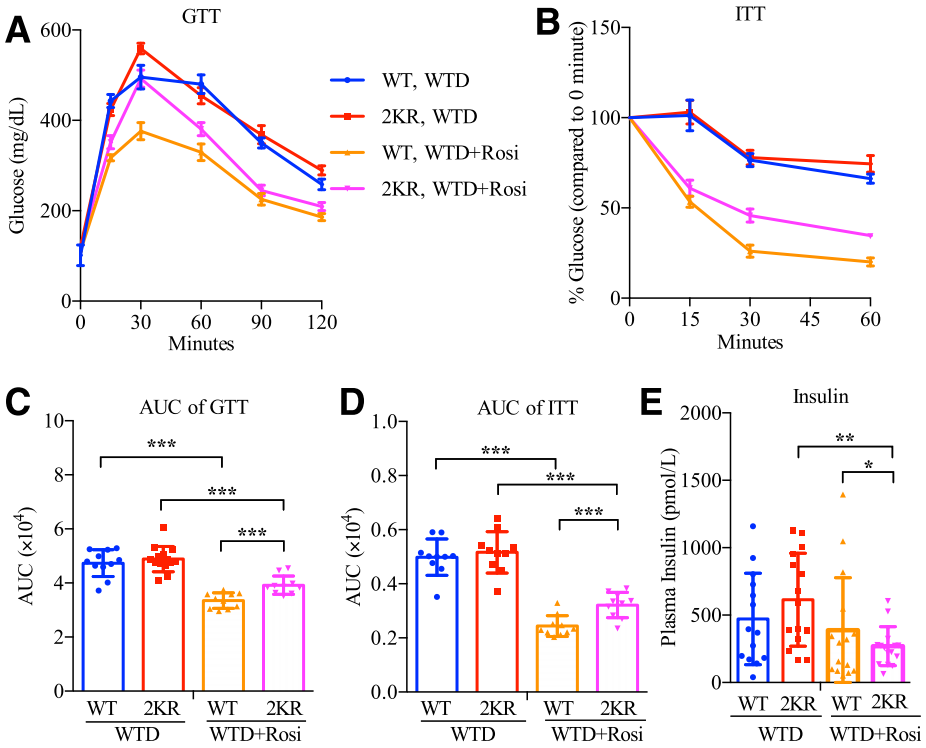

Figure 4—*2KR:Ldlr*$^{-/-}$ mice remain responsive to TZD upon insulin sensitization. Male *WT:Ldlr*$^{-/-}$ and *2KR:Ldlr*$^{-/-}$ mice were fed the WTD for 12 weeks with or without rosiglitazone treatment (11 WT and 14 2KR mice fed the WTD; 15 WT and 15 2KR mice fed the WTD and given rosiglitazone [WTD+Rosi]). *A* and *C*: Intraperitoneal glucose tolerance test (GTT) results (*A*) and the areas under the curve (AUC) (*C*). *B* and *D*: Insulin tolerance test (ITT) (*B*) and the AUC (*D*). *E*: Plasma insulin levels determined by ELISA. *$P < 0.05$, **$P < 0.01$, ***$P < 0.001$, two-way ANOVA. Data are presented as the mean ± SEM.

their mild increase in fat mass. Notably, fasting plasma insulin levels in *2KR:Ldlr*$^{-/-}$ mice were reduced more significantly than in *WT:Ldlr*$^{-/-}$ mice upon receiving rosiglitazone, indicating that they are not insulin resistant (Fig. 4*E*). In summary, *2KR:Ldlr*$^{-/-}$ mice have a largely normal response to TZDs with regard to insulin sensitization.

2KR Blunts the Adverse Effects of Rosiglitazone in an Atherogenic Model

PPARγ deacetylation uncouples the metabolic benefits of rosiglitazone from its adverse effects in diet-induced obesity (20). We investigated whether PPARγ deacetylation preserves this circumvention of TZD's side effects while conveying athero-protection in the atherogenic model. The predominant adverse effect of TZD is bone loss. Both bone volume and bone mineral density, two measures of bone strength, were significantly higher in both the trabecular and cortical regions of femurs from *2KR:Ldlr*$^{-/-}$ mice fed the WTD than those of *WT:Ldlr*$^{-/-}$ mice fed the WTD after a 12-week course of TZD treatment (Fig. 5*A*–*C*). This was associated with a striking 70% reduction of bone marrow adiposity in *2KR:Ldlr*$^{-/-}$ mice (Fig. 5*D* and *E*), in agreement with the opposite functions of PPARγ activation in bone remodeling and bone marrow adipogenesis (28). TZD also causes fluid retention with edema, which may exacerbate the risk of congestive heart failure (12,29). Rosiglitazone decreased hematocrit in *WT:Ldlr*$^{-/-}$ mice as a result of hemodilution through fluid retention. Strikingly, this decrease in hematocrit was completely prevented in *2KR:Ldlr*$^{-/-}$ mice over the course of 5 weeks (Fig. 5*F*). These results indicate that PPARγ deacetylation alleviates the adverse effects of rosiglitazone without sacrificing its ability to inhibit atherosclerosis on an *Ldlr*$^{-/-}$ background.

2KR Improves Endothelial Function

PPARγ regulates endothelial cell nitric oxide (NO) production, cell adhesion, and lipoprotein lipase activity (30–33). Genetic disruption of PPARγ in endothelial cells worsens atherosclerosis (34). Thus we interrogated the role of PPARγ deacetylation on endothelial function. It has been suggested that PPARγ can protect against atherosclerosis by regulating NO production (31) through the inhibition of inducible NO synthase (iNOS) (35) and Nox2 (36,37). Rosiglitazone can suppress iNOS (38) and Nox2 (37) expression. We therefore tested whether iNOS and Nox2 were repressed by PPARγ deacetylation. In primary endothelial cells, 2KR suppressed the expression of *iNOS*, *Nox2*, and proinflammation factor *IL6*, but it did not affect *eNOS* (Fig. 6*A*). Consistent with this, 2KR decreased levels of the Nox2 protein basally and after rosiglitazone treatment (Fig. 6*B* and *C*). We further examined the repression

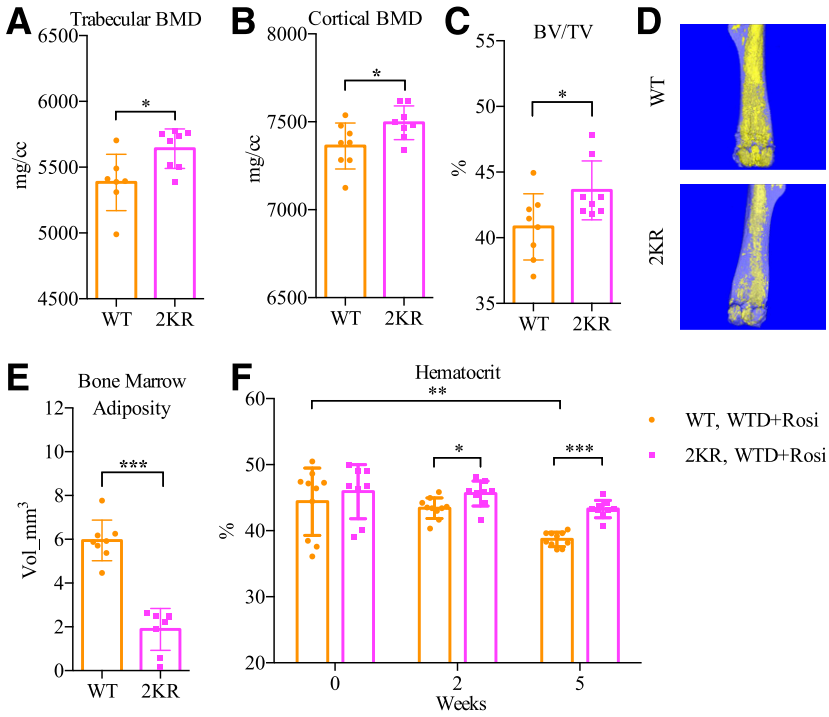

Figure 5—PPARγ deacetylation alleviates the adverse side effects of TZD on the atherogenic condition. *A–E*: Micro-CT scanning results of the femurs of male *WT:Ldlr*$^{-/-}$ (n = 8) and *2KR:Ldlr*$^{-/-}$ (n = 8) mice following 12 weeks of eating the WTD and receiving rosiglitazone treatment. *A* and *B*: Bone mineral density (BMD) in the trabecular (*A*) and cortical (*B*) areas. *C*: Relative cortex bone volume (BV)/total volume (TV). *D*: Representative images of osmium tetroxide staining of bone marrow adiposity in femurs. *E*: Quantification of femur marrow lipid volume. *$P < 0.05$, ***$P < 0.001$, WT vs. 2KR mice, two-sided Student t test. *F*: Hematocrit in male mice (10 WT and 9 2KR mice) over the course of 5 weeks of eating the WTD and receiving rosiglitazone (WTD+Rosi). *$P < 0.05$, **$P < 0.01$, ***$P < 0.001$, WT vs. 2KR mice, two-way ANOVA. Data are presented as the mean ± SEM.

of these atherogenic factors by 2KR under atherosclerosis-predisposing conditions in vivo. In aortae isolated from *WT:Ldlr*$^{-/-}$ and *2KR:Ldlr*$^{-/-}$ mice after they had eaten the WTD for 5 weeks, *iNOS*, *Nox2*, and *IL6*, but not *eNOS*, were consistently repressed in the aortae from the *2KR:Ldlr*$^{-/-}$ mice (Fig. 6*D*). Similarly, 2KR mutations reduced the amount of Nox2 protein by 70% upon WTD feeding (Fig. 6*E* and *F*). Furthermore, inflammatory markers and atherogenic factors including *Mcp1*, *F4/80*, *Nfkb*, *Icam1*, and *Vcam1* were all repressed in aortae from *2KR:Ldlr*$^{-/-}$ mice, whereas the antiatherogenic factor Nox4 (39) was induced (Fig. 6*D*). Moreover, circulating levels of interleukin-6 (IL-6) were significantly reduced in *2KR:Ldlr*$^{-/-}$ mice after 12 weeks of eating the WTD (Fig. 6*G*). Collectively, these data demonstrate that 2KR suppresses atherogenic factors in the endothelium.

Next, we asked whether this endothelium-protective effect of PPARγ deacetylation is restricted to atherogenic conditions. We isolated thoracic aortae from WT and 2KR mice eating a chow diet. PE, a vasopressor; ACh, an endothelium-dependent vasodilator; and SNP, an endothelium-independent vasodilator, were used as pharmacological tools to interrogate the vascular function of 2KR mice (23). Although both genotypes responded similarly to SNP, 2KR mice showed a significantly lower half-maximal effective concentration for ACh-induced relaxation from the PE-induced contraction than that in WT mice (Fig. 7*A–C*). Furthermore, aortae from 2KR mice exhibited a 25% enhancement in maximal relaxation in response to ACh (Fig. 7*D*). No differences in cross-sectional area and wall-to-lumen ratio were observed between WT and 2KR aortae (Fig. 7*E–G*). Together, these results indicate that 2KR mice exhibit enhanced endothelial function independent of the atherogenic condition.

DISCUSSION

Antiatherogenic Effects of PPARγ Deacetylation

Here we report an extensive analysis of the effect of PPARγ deacetylated PPARγ knock-in mice (2KR). In the *Ldlr*$^{-/-}$ mice fed the WTD, this modification reduced atherosclerotic lesion size, particularly in the aortic arch region. This antiatherogenic effect is most likely linked to the enhanced vascular endothelial function exhibited by 2KR mice, with the repression of proatherogenic and inflammatory factors, rather than changes in lipid or cholesterol levels (Fig. 8). More importantly, 2KR mice continue to respond sufficiently, albeit to a slightly smaller extent, to the insulin-sensitizing effect of TZD, without losing bone or retaining fluid. Our findings provide direct evidence

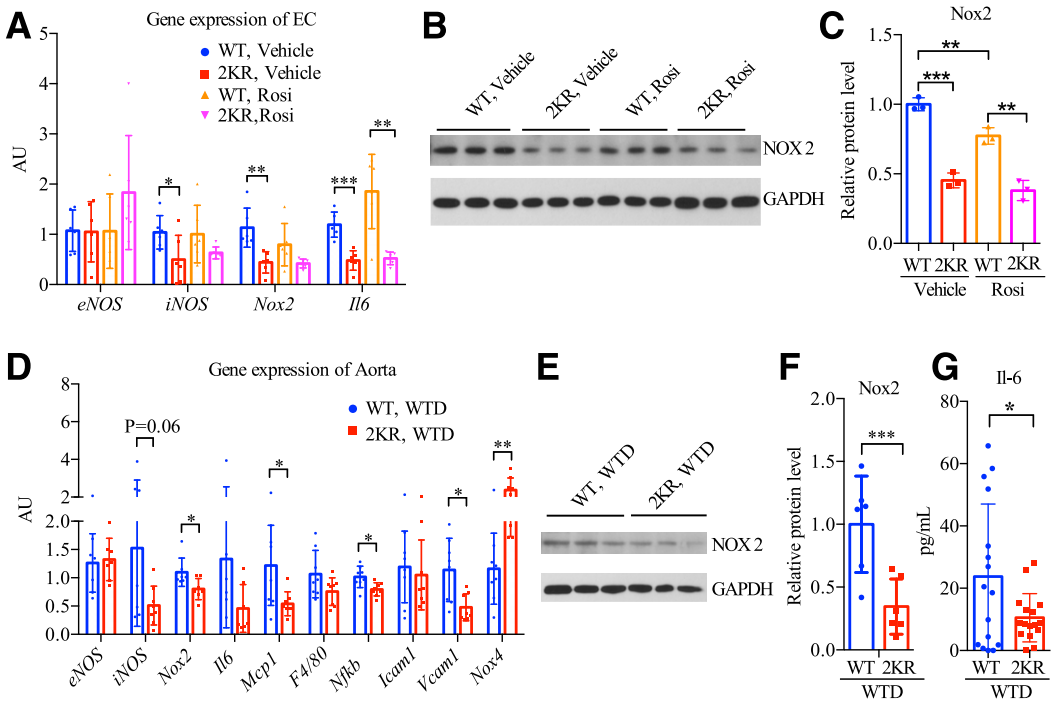

Figure 6—PPARγ deacetylation suppresses the atherogenic factors iNOS, Nox2, and IL-6 in the endothelium. *A–C*: Primary lung endothelial cells (ECs) were isolated from *WT:Ldlr*$^{-/-}$ and *2KR:Ldlr*$^{-/-}$ mice and treated with a vehicle or 1 μmol/L rosiglitazone (Rosi) for 12 h after confluence. *A*: Quantitative PCR analysis of endothelial gene expression (n = 6 mice per group). *B* and *C*: Western blotting (*B*) and quantification (n = 3) (*C*) of Nox2 in primary lung ECs. *D–F*: Male *WT:Ldlr*$^{-/-}$ and *2KR:Ldlr*$^{-/-}$ mice were fed the WTD for 5 weeks. *D*: Quantitative PCR analysis of gene expression in the aortae (n = 7 mice per group). *E*: Representative Western blotting of Nox2 in the aortae. *F*: Quantification of Nox2 normalized to GAPDH (n = 6 mice per group). *G*: Plasma IL-6 in male mice (n = 16 per group) fed the WTD for 12 weeks. *$P < 0.05$, **$P < 0.01$, ***$P < 0.001$, WT vs. 2KR mice, two-sided Student t test. Data are presented as the mean ± SEM.

that agents modifying PPARγ acetylation hold promise for the combined treatment of CVD and type 2 diabetes (20,40,41).

Unmasking Effects of PPARγ Deacetylation on Lipid and Lipoprotein Metabolism

The *Ldlr*$^{-/-}$ model used to analyze the effect of the 2KR mutation potentially overlooks contributions of PPARγ deacetylation to lipid turnover and lipoprotein metabolism, owing to the overwhelming effects of Ldlr knockout combined with WTD consumption. Indeed, we previously showed an improved lipid profile in 2KR mice fed an HFD (20). In the current study, we observed signs of improved lipid and cholesterol metabolism with rosiglitazone treatment but not under basal conditions. The disruption of lipoprotein uptake in the *Ldlr*$^{-/-}$ model may also underpin the lesser weight the mice gained upon eating the WTD, besides the dietary difference (42% fat in the WTD vs. 60% fat in the HFD). This less obesity-prone condition may diminish the benefit of 2KR on inhibiting weight gain, as seen in DIO mice (20). Indeed, *2KR:Ldlr*$^{-/-}$ mice mimicked the effect of TZD in mobilizing lipids from the liver for storage in subcutaneous adipose tissue (24), resulting in a mild increase in adipose mass. Future investigation is desired to understand the potential regulation of lipid and cholesterol metabolism by PPARγ deacetylation and its effect on atherosclerosis. To this end, other models with preserved residual LDL receptor function, such as AAV8-PCSK9 D377Y-mediated LDL receptor degradation, should be used (42).

Vascular Endothelial Function and PPARγ Deacetylation

The improvement in vascular function caused by 2KR is consistent with the protective role of PPARγ in the vasculature. PPARγ isoform 1 is abundant in endothelial cells, and its activation represses downstream targets of nuclear factor-κB, including iNOS, vascular cell adhesion molecule-1, and intracellular adhesion molecule-1, which regulate cellular adhesion and inflammation. We observed a significant decrease of iNOS in 2KR aortae and in primary endothelial cells, together with the repression of the atherogenic factor Nox2 and inflammatory IL-6. The transrepression function of PPARγ involves ligand-dependent SUMOylation of K365 (K395 on PPARγ2) to retain corepressor complexes on inflammatory gene promoters (15). Interestingly, target residues of ligand-dependent deacetylation, K268 and K293 (on PPARγ2), are located within the same domain as K395, with the three lysines surrounding a β-sheet at the back wall of the ligand-binding pocket (Supplementary Fig. 4*A* and *B*).

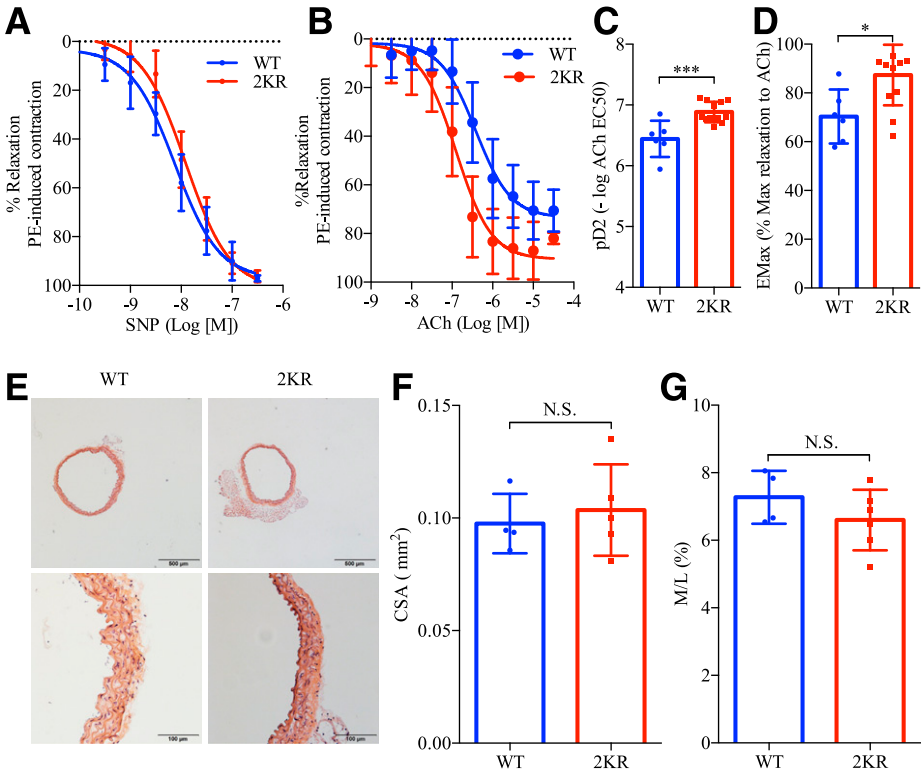

Figure 7—PPARγ deacetylation enhances endothelial function in aortae from 8-week-old male mice. *A*: Curves of endothelium-independent relaxation in response to SNP (1 nmol/L to 10 μmol/L) (6 WT mice, 10 2KR mice). *B*: Curves of endothelium-dependent relaxation in response to ACh (1 nmol/L to 10 μmol/L) (8 WT mice, 13 2KR mice). *C*: Vascular sensitivity, plotted as pD2 (−log of the half-maximal effective concentration [EC_{50}]) of Ach (6 WT mice, 12 2KR mice). *D*: Maximum aortic relaxation in response to ACh in male mice (6 WT mice, 12 2KR mice). *E*: Representative images of aortae from WT and 2KR mice stained with H&E (magnification ×4 [top] and ×20 [bottom]). *F* and *G*: Measurements of the cross-sectional area (CSA) (*F*) and media-to-lumen ratio (M/L) (*G*). $^*P < 0.05$, $^{***}P < 0.001$, WT vs. 2KR mice, two-sided Student *t* test. Data are presented as the mean ± SEM. N.S., not significant.

Notably, K395 is buried inside the structure, in contrast to K268 and K293, which are exposed on the surface. Thus, it is plausible that K268 and K293 are more accessible to modifying enzymes, and their TZD-dependent deacetylation facilitates the SUMOylation of K395. The balance between deacetylation and SUMOylation is likely important in the context of transrepression of inflammatory genes. Furthermore, the vasculoprotective effect of 2KR is in line with the anti-inflammatory function of SIRT1, an important PPARγ deacetylase, in endothelial cells (19,43,44). Studies using endothelial-specific PPARγ deacetylation models will be needed to delineate the effects of deacetylated PPARγ in endothelial cells and its contribution to the antiatherogenic phenotype.

Perivascular Fat and Antiatherogenic Effects of PPARγ Deacetylation

There are several potential explanations for the observation that the 2KR mutants have a more pronounced antiatherogenic effect at the aortic arch than at the root. Atherosclerotic plaques are more frequently found near bifurcation and highly curved areas, typically the aortic arch (45,46). This proneness to atherosclerosis at the aortic arch is often related to the hemodynamic stress on vascular endothelium (47,48), a prominent connection between diabetes and atherosclerosis (49). In this context, the more pronounced antiatherogenic effect of 2KR in the aortic arch is consistent with improved endothelial function rather than the lipid profile. Another possibility is that the difference reflects a contribution from perivascular fat, which is more abundant at the arch than at the root. This fat has been demonstrated to be closely associated with atherosclerotic plaque development, and its depletion by targeted PPARγ ablation worsens atherosclerosis (50). Perivascular fat at the arch consists of brown adipocytes, which undergo dynamic remodeling. Cold challenge activates its thermogenic response and decreases plaque development, whereas thermoneutrality mimics high-fat feeding and suppresses its brown adipocyte features, resulting in worse atherosclerosis (50). Of note, PPARγ deacetylation underlies the browning function of TZDs, and 2KR mice show brown remodeling of WAT in addition to increased energy expenditure (20). Therefore, preserving the brown feature of perivascular fat may be another mechanism underpinning the protection of *2KR:Ldlr*$^{-/-}$ mice from atherosclerosis.

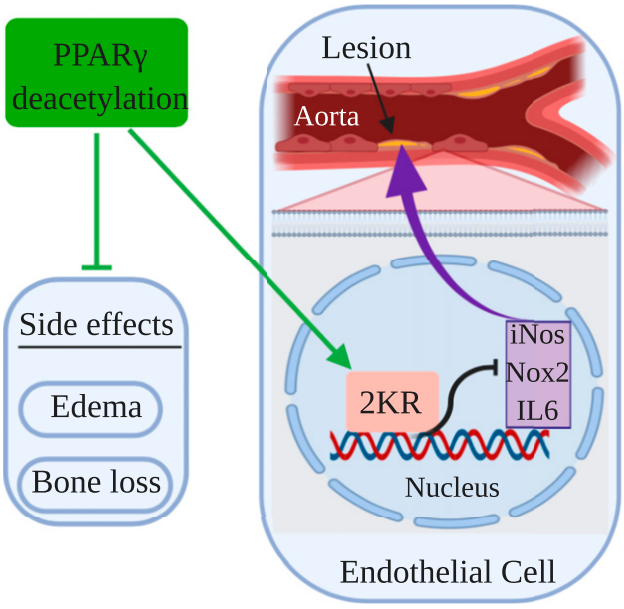

Figure 8—Model of PPARγ deacetylation that confers the antiatherogenic effect and improves endothelial function with diabetes treatment. Aortic arch lesion size reduced by 2KR through suppression of iNOS, Nox2, and IL-6 in endothelial cells while circumventing the side effects of TZD, including fluid retention and bone loss.

In summary, our findings suggest a dual effect of PPARγ deacetylation: under basal conditions, in the absence of TZDs, it induces a moderate gain of PPARγ function that mimics the effects of TZD to decrease atherosclerosis; upon TZD treatment, it selectively activates PPARγ targets, retaining insulin sensitization and an antiatherogenic effect while preventing bone loss and fluid retention. As PPARγ has pleiotropic effects on tissues that are relevant to cardiometabolic health, its integrative antiatherosclerotic function may also entail improvements in dyslipidemia, endothelial function, and brown remodeling of perivascular fat. We envision that our findings on the role of PPARγ deacetylation on atherosclerosis will incite new avenues for developing drugs for treating atherosclerosis in people with type 2 diabetes, which could include manipulation of PPARγ acetylation or compounds binding to this very flexible hinge region containing K268 and K293 to exert transcriptional selectivity.

Acknowledgments. The authors thank G. Kuriakose and S.E. Abramowicz at the Atherosclerosis Phenotyping Core, Department of Medicine of Columbia University, for analyzing atherosclerotic plaque; A.M. Flete and T. Kolar, Department of Medicine of Columbia University, for providing technical assistance with animal studies; and Z. Li at SUNY Downstate Medical Center for providing technical support for aorta dissection.

Funding. This work was supported by the National Institutes of Health (grants R00DK97455 and R01DK112943 [to L.Q.], and grant P01HL087123 [to D.A. and L.Q.]).

The content is solely the responsibility of the authors and does not necessarily represent the official views of the National Institutes of Health.

Duality of Interest. No potential conflicts of interest relevant to this article were reported.

Author Contributions. L.L., L.F., M.J.K., and M.A.C.-S. developed the methodology. L.L., L.F., M.C., M.J.K., J.Y., Y.F., N.A., Q.W., and M.A.C.-S. performed the investigation. L.L. wrote the original draft of the manuscript. M.C., A.R.T., I.T., D.A., and L.Q. reviewed and edited the manuscript. D.A. and L.Q. conceptualized the study. L.Q. is the guarantor of this work and, as such, had full access to all the data in the study and takes responsibility for the integrity of the data and the accuracy of the data analysis.

References

1. Giorda CB, Avogaro A, Maggini M, et al.; Diabetes and Informatics Study Group. Recurrence of cardiovascular events in patients with type 2 diabetes: epidemiology and risk factors. Diabetes Care 2008;31:2154–2159
2. Caro JJ, Ward AJ, O'Brien JA. Lifetime costs of complications resulting from type 2 diabetes in the U.S. Diabetes Care 2002;25:476–481
3. Després JP, Lamarche B, Mauriège P, et al. Hyperinsulinemia as an independent risk factor for ischemic heart disease. N Engl J Med 1996;334:952–957
4. Tontonoz P, Graves RA, Budavari AI, et al. Adipocyte-specific transcription factor ARF6 is a heterodimeric complex of two nuclear hormone receptors, PPAR gamma and RXR alpha. Nucleic Acids Res 1994;22:5628–5634
5. Tontonoz P, Spiegelman BM. Fat and beyond: the diverse biology of PPARgamma. Annu Rev Biochem 2008;77:289–312
6. Lehrke M, Lazar MA. The many faces of PPARgamma. Cell 2005;123:993–999
7. Li AC, Brown KK, Silvestre MJ, Willson TM, Palinski W, Glass CK. Peroxisome proliferator-activated receptor gamma ligands inhibit development of atherosclerosis in LDL receptor-deficient mice. J Clin Invest 2000;106:523–531
8. Kintscher U, Goetze S, Wakino S, et al. Peroxisome proliferator-activated receptor and retinoid X receptor ligands inhibit monocyte chemotactic protein-1-directed migration of monocytes. Eur J Pharmacol 2000;401:259–270
9. Subramanian V, Golledge J, Ijaz T, Bruemmer D, Daugherty A. Pioglitazone-induced reductions in atherosclerosis occur via smooth muscle cell-specific interaction with PPARgamma. Circ Res 2010;107:953–958
10. Kernan WN, Viscoli CM, Furie KL, et al.; IRIS Trial Investigators. Pioglitazone after ischemic stroke or transient ischemic attack. N Engl J Med 2016;374:1321–1331
11. Qiang L, Accili D. FGF21 and the second coming of PPARγ. Cell 2012;148:397–398
12. Soccio RE, Chen ER, Lazar MA. Thiazolidinediones and the promise of insulin sensitization in type 2 diabetes. Cell Metab 2014;20:573–591
13. Iankova I, Petersen RK, Annicotte JS, et al. Peroxisome proliferator-activated receptor gamma recruits the positive transcription elongation factor B complex to activate transcription and promote adipogenesis. Mol Endocrinol 2006;20:1494–1505
14. Choi JH, Banks AS, Estall JL, et al. Anti-diabetic drugs inhibit obesity-linked phosphorylation of PPARgamma by Cdk5. Nature 2010;466:451–456
15. Pascual G, Fong AL, Ogawa S, et al. A SUMOylation-dependent pathway mediates transrepression of inflammatory response genes by PPAR-gamma. Nature 2005;437:759–763
16. Ji S, Park SY, Roth J, Kim HS, Cho JW. O-GlcNAc modification of PPARγ reduces its transcriptional activity. Biochem Biophys Res Commun 2012;417:1158–1163
17. Choi JH, Banks AS, Kamenecka TM, et al. Antidiabetic actions of a non-agonist PPARγ ligand blocking Cdk5-mediated phosphorylation. Nature 2011;477:477–481
18. Stechschulte LA, Czernik PJ, Rotter ZC, et al. PPARG post-translational modifications regulate bone formation and bone resorption. EBioMedicine 2016;10:174–184
19. Qiang L, Wang L, Kon N, et al. Brown remodeling of white adipose tissue by SirT1-dependent deacetylation of Pparγ. Cell 2012;150:620–632
20. Kraakman MJ, Liu Q, Postigo-Fernandez J, et al. PPARγ deacetylation dissociates thiazolidinedione's metabolic benefits from its adverse effects. J Clin Invest 2018;128:2600–2612

21. Liu Q, Yu J, Wang L, et al. Inhibition of PU.1 ameliorates metabolic dysfunction and non-alcoholic steatohepatitis. J Hepatol. 3 March 2020 [Epub ahead of print]. DOI: 10.1016/j.jhep.2020.02.02532135178
22. Fredman G, Kamaly N, Spolitu S, et al. Targeted nanoparticles containing the proresolving peptide Ac2-26 protect against advanced atherosclerosis in hypercholesterolemic mice [published correction appears in Sci Transl Med 2015; 7:277er2]. Sci Transl Med 2015;7:275ra20
23. Kramer B, França LM, Zhang Y, Paes AMA, Gerdes AM, Carrillo-Sepulveda MA. Western diet triggers Toll-like receptor 4 signaling-induced endothelial dysfunction in female Wistar rats. Am J Physiol Heart Circ Physiol 2018;315: H1735–H1747
24. Juurinen L, Kotronen A, Granér M, Yki-Järvinen H. Rosiglitazone reduces liver fat and insulin requirements and improves hepatic insulin sensitivity and glycemic control in patients with type 2 diabetes requiring high insulin doses. J Clin Endocrinol Metab 2008;93:118–124
25. Tall AR, Yvan-Charvet L, Terasaka N, Pagler T, Wang N. HDL, ABC transporters, and cholesterol efflux: implications for the treatment of atherosclerosis. Cell Metab 2008;7:365–375
26. Shea S, Stein JH, Jorgensen NW, et al. Cholesterol mass efflux capacity, incident cardiovascular disease, and progression of carotid plaque. Arterioscler Thromb Vasc Biol 2019;39:89–96
27. Sakamoto J, Kimura H, Moriyama S, et al. Activation of human peroxisome proliferator-activated receptor (PPAR) subtypes by pioglitazone. Biochem Biophys Res Commun 2000;278:704–711
28. Wei W, Wan Y. Thiazolidinediones on PPARγ: the roles in bone remodeling. PPAR Res 2011;2011:867180
29. Ahmadian M, Suh JM, Hah N, et al. PPARγ signaling and metabolism: the good, the bad and the future. Nat Med 2013;19:557–566
30. Matsumoto M, Pocai A, Rossetti L, Depinho RA, Accili D. Impaired regulation of hepatic glucose production in mice lacking the forkhead transcription factor Foxo1 in liver. Cell Metab 2007;6:208–216
31. Calnek DS, Mazzella L, Roser S, Roman J, Hart CM. Peroxisome proliferator-activated receptor gamma ligands increase release of nitric oxide from endothelial cells. Arterioscler Thromb Vasc Biol 2003;23:52–57
32. Jackson SM, Parhami F, Xi XP, et al. Peroxisome proliferator-activated receptor activators target human endothelial cells to inhibit leukocyte-endothelial cell interaction. Arterioscler Thromb Vasc Biol 1999;19:2094–2104
33. Kanda T, Brown JD, Orasanu G, et al. PPARgamma in the endothelium regulates metabolic responses to high-fat diet in mice. J Clin Invest 2009;119: 110–124
34. Qu A, Shah YM, Manna SK, Gonzalez FJ. Disruption of endothelial peroxisome proliferator-activated receptor γ accelerates diet-induced atherogenesis in LDL receptor-null mice. Arterioscler Thromb Vasc Biol 2012;32:65–73
35. Chen CW, Chang YH, Tsi CJ, Lin WW. Inhibition of IFN-gamma-mediated inducible nitric oxide synthase induction by the peroxisome proliferator-activated receptor gamma agonist, 15-deoxy-delta 12,14-prostaglandin J2, involves inhibition of the upstream Janus kinase/STAT1 signaling pathway. J Immunol 2003;171:979–988
36. Quesada IM, Lucero A, Amaya C, et al. Selective inactivation of NADPH oxidase 2 causes regression of vascularization and the size and stability of atherosclerotic plaques. Atherosclerosis 2015;242:469–475
37. Hwang J, Kleinhenz DJ, Rupnow HL, et al. The PPARgamma ligand, rosiglitazone, reduces vascular oxidative stress and NADPH oxidase expression in diabetic mice. Vascul Pharmacol 2007;46:456–462
38. Betz B, Schneider R, Kress T, Schick MA, Wanner C, Sauvant C. Rosiglitazone affects nitric oxide synthases and improves renal outcome in a rat model of severe ischemia/reperfusion injury. PPAR Res 2012;2012:219319
39. Schürmann C, Rezende F, Kruse C, et al. The NADPH oxidase Nox4 has anti-atherosclerotic functions. Eur Heart J 2015;36:3447–3456
40. Quelle FW, Sigmund CD. PPARγ: no SirT, no service. Circ Res 2013;112:411–414
41. Lazar MA. Reversing the curse on PPARγ. J Clin Invest 2018;128:2202–2204
42. Bjørklund MM, Hollensen AK, Hagensen MK, et al. Induction of atherosclerosis in mice and hamsters without germline genetic engineering. Circ Res 2014;114:1684–1689
43. Jia Y, Gao P, Chen H, et al. SIRT1 suppresses PMA and ionomycin-induced ICAM-1 expression in endothelial cells. Sci China Life Sci 2013;56:19–25
44. Potente M, Ghaeni L, Baldessari D, et al. SIRT1 controls endothelial angiogenic functions during vascular growth. Genes Dev 2007;21:2644–2658
45. Qiang L, Banks AS, Accili D. Uncoupling of acetylation from phosphorylation regulates FoxO1 function independent of its subcellular localization. J Biol Chem 2010;285:27396–27401
46. Fox B, Seed WA. Location of early atheroma in the human coronary arteries. J Biomech Eng 1981;103:208–212
47. LaMack JA, Himburg HA, Friedman MH. Distinct profiles of endothelial gene expression in hyperpermeable regions of the porcine aortic arch and thoracic aorta. Atherosclerosis 2007;195:e35–e41
48. Hastings NE, Simmers MB, McDonald OG, Wamhoff BR, Blackman BR. Atherosclerosis-prone hemodynamics differentially regulates endothelial and smooth muscle cell phenotypes and promotes pro-inflammatory priming. Am J Physiol Cell Physiol 2007;293:C1824–C1833
49. Liu Z. The vascular endothelium in diabetes and its potential as a therapeutic target. Rev Endocr Metab Disord 2013;14:1–3
50. Chang L, Villacorta L, Li R, et al. Loss of perivascular adipose tissue on peroxisome proliferator-activated receptor-γ deletion in smooth muscle cells impairs intravascular thermoregulation and enhances atherosclerosis. Circulation 2012;126:1067–1078